Anisotropic optical conductivities due to spin and orbital ordering in $LaVO_3$ and YVO_3: First-principles studies

Zhong Fang
Tokura Spin Superstructure Project (SSS), ERATO, Japan Science and Technology Corporation (JST), c/o National Institute of Advanced Industrial Science and Technology (AIST), Tsukuba Central 4, 1-1-1 Higashi, Tsukuba, Ibaraki 305-8562, Japan

Naoto Nagaosa
Correlated Electron Research Center (CERC), AIST Tsukuba Central 4, 1-1-1 Higashi, Tsukuba, Ibaraki 305-8562, Japan and Department of Applied Physics, University of Tokyo, 7-3-1, Hongo, Bunkyo-ku, Tokyo 113-8656, Japan

Kiyoyuki Terakura
Research Institute for Computational Sciences (RICS), AIST Tsukuba Central 2, 1-1-1 Umezono, Tsukuba, Ibaraki 305-8568, Japan
(Received 7 August 2002; published 6 January 2003)

The anisotropy of low-energy ($0\sim5$ eV) optical excitations in strongly correlated transition-metal oxides is closely related to the spin and orbital orderings. The recent successes of LDA+U method in describing the magnetic and electronic structures enable us to calculate the optical conductivity from first principles. The $LaVO_3$ and YVO_3, both of which have $3d^2$ configuration and have various spin and orbital ordered phases at low temperature, show distinct anisotropy in the optical spectra. The effects of spin and orbital ordering on the anisotropy are studied in detail based on our first-principles calculations. The experimental spectra of both compounds at low-temperature phases can be qualitatively explained with our calculations, while the studies for the intermediate temperature phase of YVO_3 suggest the substantial persistence of the low-temperature phase at elevated temperature.

DOI: 10.1103/PhysRevB.67.035101 PACS number(s): 75.30.−m, 78.20.Bh, 71.27.+a

I. INTRODUCTION

The strong couplings among the spin, lattice, and charge degrees of freedom in transition-metal oxides are essentially mediated by the orbital degree of freedom, which plays a crucial role in controlling the phases and various physical properties.[1–3] The direct observation of orbital structure is difficult, yet several experiments[4–6] have been developed to detect the anisotropy induced by spin and orbital orderings. Among them, the measurement of anisotropic optical conductivity[5,6] by using polarized light can provide us with useful information. The low-energy optical excitations below the strong O $2p$ to transition-metal $3d$ charge-transfer peak mostly come from the transition-metal $3d$-to-$3d$ transitions. Those transitions reflect sensitively the spin and orbital structures of the system through optical transition-matrix elements, and show anisotropy when spin and orbital are cooperatively ordered.[7,8] Nevertheless, the proper analysis of experimental anisotropic optical spectra requires the detailed understanding of electronic and magnetic structures.

Both $LaVO_3$ and YVO_3 are insulators with a $Pbnm$ orthorhombic unit cell with $a\approx b\approx c/\sqrt{2}$ at room temperature. There are two $3d$ electrons per V^{3+} site. Synchrotron x-ray and neutron diffraction results[9] suggested that $LaVO_3$ undergoes a magnetic phase transition at 143 K (Ref. 10) and a structural phase transition at 140 K. The low-temperature phase has the *C*-type antiferromagnetic (AF) spin configuration (i.e., ferromagnetic (FM) coupling along the c axis and AF coupling in the a-b plane). Due to the Jahn-Teller distortion, one of the V—O bond is longer than other two in the VO_6 octahedron. The longer bond lies in the a-b plane and its orientation alternates for the neighboring V sites in the plane. The stacking of the longer bonds also alternates along the c axis. Hereafter, we call this kind of distortion the *G*-type Jahn-Teller distortion. This low-temperature phase has $P2_1/a$ crystal symmetry.

The structural and magnetic phases for YVO_3 are quite complicated.[11–13] With lowering the temperature, this compound first undergoes a structural phase transition at 200 K from a disordered phase to the *G*-type Jahn-Teller distorted structure, the same structure as the low-temperature phase of $LaVO_3$. Then the *C*-type AF ordering develops at 116 K (T_{N1}). With further lowering the temperature to 77 K (T_{N2}), another structural and magnetic phase appears. The low-temperature (<77 K) phase recovers the $Pbnm$ crystal symmetry with the *C*-type Jahn-Teller distortion (i.e., the longer bonds stack along the c axis in the same orientation rather than alternately). The magnetic structure of this low-temperature phase is *G*-type AF structure (i.e., AF coupling both in the a-b plane and along the c axis). Strong temperature-induced magnetization reversal can be observed at T_{N1} and T_{N2}.[14]

Sawada and Terakura studied the electronic and magnetic structures of $LaVO_3$ and YVO_3 by using the full-potential linearized augmented-plane-wave method. They first compared the results[15] between LDA (local density approximation) and GGA (generalized gradient approximation), and then applied the LDA+U method[16] to $LaVO_3$.[17] They found that the LDA and GGA are not sufficient, and LDA+U is necessary in order to predict the low-temperature phase correctly. Recently, the polarized optical conductivities of $LaVO_3$ and YVO_3 were measured by Miyasaka *et al.*[18] and

very clear anisotropy was observed. To understand the implications of those spectra, we developed the plane-wave pseudopotential method based on LDA+U to calculate the optical conductivity and studied the effects of spin and orbital orderings on the anisotropy. The experimental spectra of both $LaVO_3$ and YVO_3 at low-temperature can be qualitatively explained by our calculations, while the studies for the intermediate temperature phase ($77\ \mathrm{K} < T < 116\ \mathrm{K}$) for YVO_3 suggest the complication of magnetic and orbital structures. In Sec. II of this paper, we will describe our method, and the results are discussed in Sec. III.

II. METHOD

The Vanderbilt type ultrasoft pseudopotential[19] is useful not only for efficient calculations for transition-metal oxides but also for implementing the LDA+U method to treat effects of strong correlation. In the LDA+U method, the strong Coulomb interaction is explicitly taken into account in the subspace of localized orbitals through a Harteree-like scheme. The detailed description of our LDA+U scheme was given in Ref. 3.

The interband optical conductivity is calculated from the converged Kohn-Sham wave functions $|\psi_{n\mathbf{k}}\rangle$ and eigen values $E_n(\mathbf{k})$ by using the following Kubo formula[20] (in Ry units):

$$\sigma_{\alpha\beta}(\omega) = -\frac{16}{V}\sum_{\mathbf{k}n} i f_{n\mathbf{k}} \sum_{m} \frac{1}{\omega_{mn}^2 - (\omega + i\delta)^2} \times \left[\frac{\omega + i\delta}{\omega_{mn}} \mathrm{Re}(\pi_{nm}^{\alpha}\pi_{mn}^{\beta}) + i\,\mathrm{Im}(\pi_{nm}^{\alpha}\pi_{mn}^{\beta}) \right], \quad (1)$$

where α and $\beta(=x,y,z)$ are indices for directions, ω is the excitation energy, V is the volume of the unit cell, n and m are band indices, $f_{n\mathbf{k}}$ is the Fermi distribution function, $\omega_{mn} = E_m(\mathrm{k}) - E_n(\mathrm{k})$ and δ is the lifetime broadening ($\delta = 0.01$ Ry in this work), $\pi_{nm}^{\alpha} = \langle \psi_{n\mathbf{k}} | (-i\nabla_{\alpha}) | \psi_{m\mathrm{k}} \rangle$ are the matrix elements of the momentum operator. The calculations for the matrix elements π_{nm}^{α} require the all electron wavefunctions $\psi_{n\mathbf{k}}$, which can be obtained from the following core compensation form:[21,22]

$$|\psi_{n\mathbf{k}}\rangle = |\phi_{n\mathbf{k}}\rangle + \sum_i \{|\psi_i\rangle - |\phi_i\rangle\}\langle\beta_i|\phi_{n\mathbf{k}}\rangle, \quad (2)$$

where $\phi_{n\mathbf{k}}$ are the pseudo-wave functions obtained from the self-consistent pseudopotential calculations, i is the index for

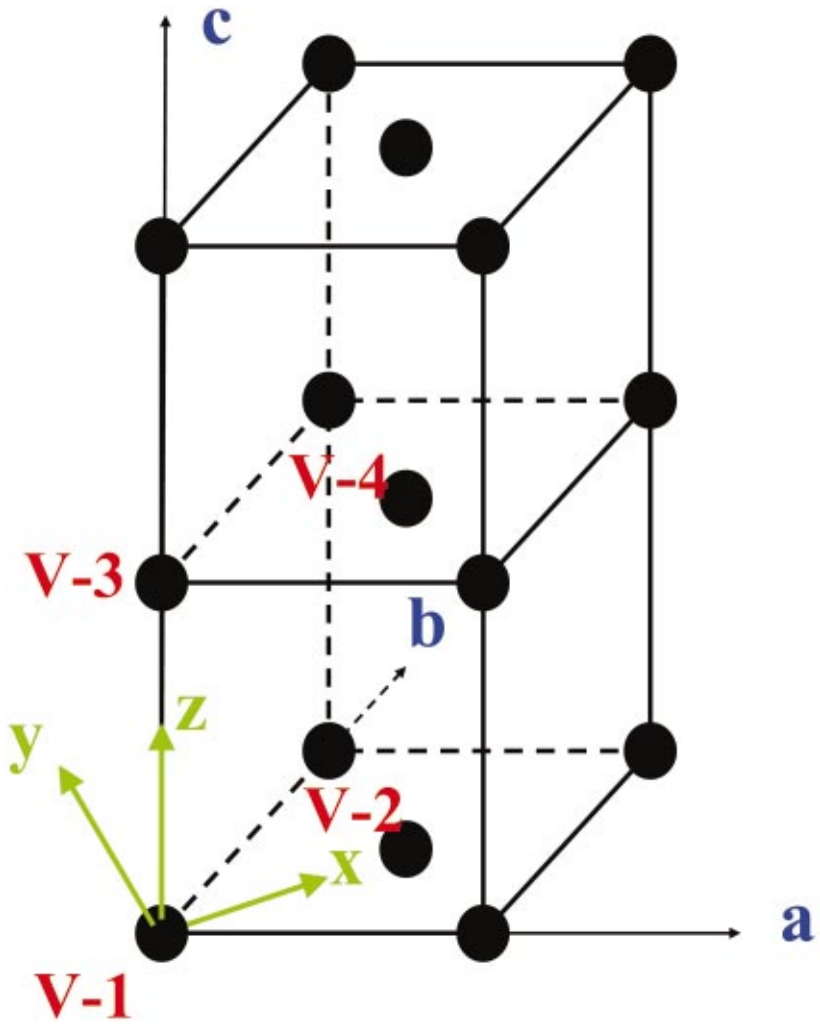

FIG. 1. (Color) The unit cell and coordinates used in the calculations. Four V sites (black spheres), labeled as V-1, V-2, V-3, and V-4, are included in the unit cell.

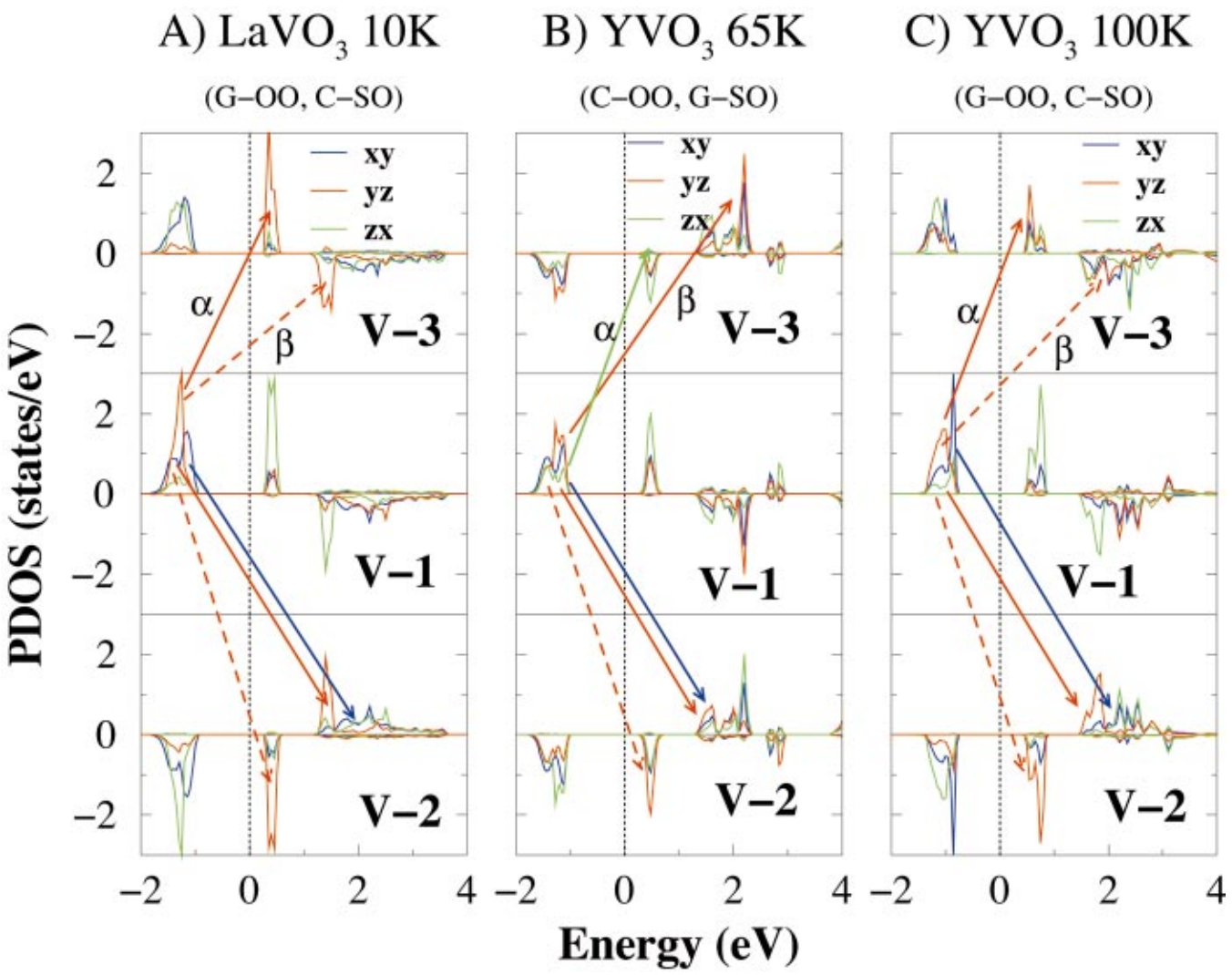

FIG. 2. (Color) The calculated projected densities of states (PDOS) for the lowest-energy states of three systems. They are (a) $LaVO_3$ 10 K structure with *G*-OO and *C*-SO; (b) YVO_3 65 K structure with *C*-OO and *G*-SO; (c) YVO_3 100 K structure with *G*-OO and *C*-SO. The lines with arrow indicate the optical transition paths from V-1 site to other sites. All the PDOS and paths for different orbitals are indicated by different colors. The solid arrows show the real transition in this spin and orbital configuration, while the dashed arrows show the possible transition in different magnetic structures. The positive and negative PDOS values mean ↑-spin and ↓-spin, respectively. See the text for detailed explanations.

atomic orbitals, ψ_i and ϕ_i are atomic all-electron and pseudo- wave functions respectively, β_i are the localized functions as defined in Ref. 19. Therefore, the matrix elements of momentum operator can be obtained as:[21,22]

$$\pi^{\alpha}_{nm} = \langle \psi_{n\mathbf{k}} | (-i\nabla_{\alpha}) | \psi_{m\mathbf{k}} \rangle = \langle \phi_{n\mathbf{k}} | (-i\nabla_{\alpha}) | \phi_{m\mathbf{k}} \rangle + \sum_{ij} \langle \phi_{n\mathbf{k}} | \beta_i \rangle \{ \langle \psi_i | (-i\nabla_{\alpha}) | \psi_j \rangle - \langle \phi_i | (-i\nabla_{\alpha}) | \phi_j \rangle \} \times \langle \beta_j | \phi_{m\mathbf{k}} \rangle. \quad (3)$$

Practically, the core contribution [second term of Eq. (3)] can be calculated in the pseudopotential generation process and stored as input of self-consistent calculations. The present process has been well checked by using $LaMnO_3$ as an example.[7,8] Throughout the calculations, 30 Ry has been used for the cutoff energy of plane-wave expansion, and we use $(6\times6\times4)$ mesh for the **k**-points in the linear tetrahedron method with the curvature correction. The parameter U_{eff} in LDA+U scheme is chosen to be about 3.0 eV in order to reproduce the experimental band gaps.[3,18,23]

III. RESULTS AND DISCUSSIONS

A. Electronic structures

The unit cell and coordinates are defined in Fig. 1. Four V atoms, say V-1, V-2, V-3, and V-4, are included in the unit cell. Following the common convention, we defined the *x*, *y*, and *z* directions as the [110], [$\bar{1}$10], and [001] directions of the unit cell respectively. Three structures, $LaVO_3$ at 10 K,[9] YVO_3 at 65 K,[13] and YVO_3 at 100 K (Ref. 13) are treated here, which have the *G*-type, *C*-type, and *G*-type Jahn-Teller

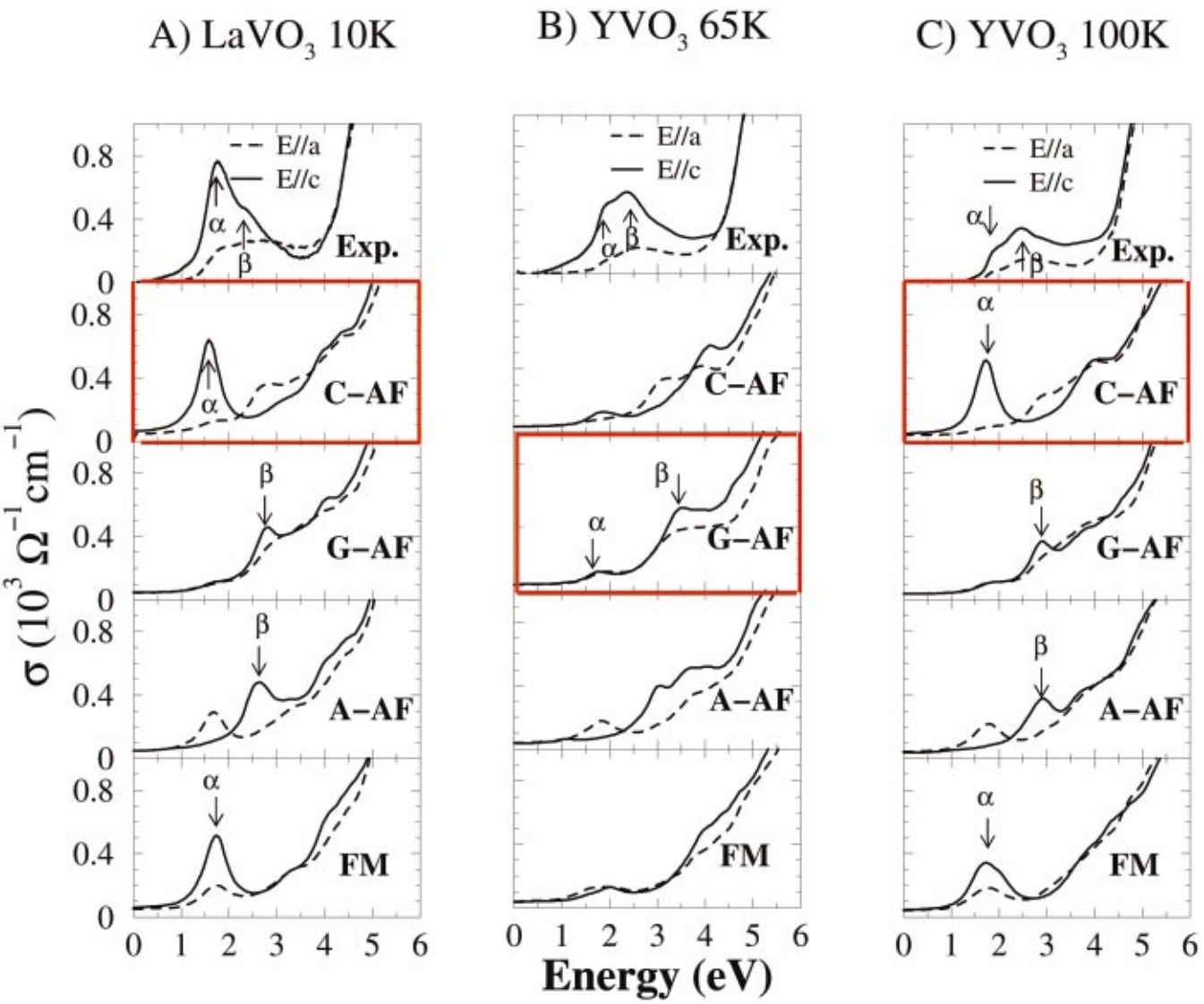

FIG. 3. (Color) The calculated optical conductivities for various phases. Three structures, (a) $LaVO_3$ at 10 K, (b) YVO_3 at 65 K, and (c) YVO_3 at 100 K, are calculated. For each fixed structure, results for four different magnetic configurations are plotted together with experimental results. The figure enclosed by the red border line corresponds to the most stable spin structure. The experimental curves in (a), (b), and (c) are taken at 10 K, 67 K, and 110 K, respectively.[18] The solid lines are results for $E//c$, while dashed lines for $E//a$. See the text for the detailed explanations.

distortions, respectively. For each fixed structure, relative stability is studied among four kinds of collinear magnetic structures: *C*-type AF, *G*-type AF, *A*-type AF(i.e., FM layers coupled antiferromagneticaly along the *c* axis), and FM spin ordering (SO) states.

Each of the above Jahn-Teller distortions is accompanied by the same type of orbital ordering (OO) and stabilizes a specific related magnetic structure. In the present case, our calculations suggest that the *G*-type and *C*-type OO favor the *C*-type and *G*-type AF SO, respectively. This result is consistent with experimental observations and also with the previous calculations[15,17] and unrestricted Hartree-Fock studies.[24] Now we concentrate on the discussion for the electronic structures of the lowest-energy magnetic state of each structure. They are (a) $LaVO_3$ 10 K with *G*-OO and *C*-SO; (b) YVO_3 65 K with *C*-OO and *G*-SO; (c) YVO_3 100 K with *G*-OO and *C*-SO. The obtained magnetic moments for these three states are all about $1.7\mu_B$/V. The calculated electronic projected densities of states (PDOS) are summarized in Fig. 2, where different orbitals are shown by different colors. The O-2*p* and V-e_g states are not plotted.

For (a), the occupied electronic configuration can be nominally expressed as V-1: $d^{\uparrow}_{xy}d^{\uparrow}_{yz}$; V-2: $d^{\downarrow}_{xy}d^{\downarrow}_{zx}$; V-3: $d^{\uparrow}_{xy}d^{\uparrow}_{zx}$; V-4: $d^{\downarrow}_{xy}d^{\downarrow}_{yz}$. One of the two electrons on each V site will occupy the d_{xy} orbital, and another electron will occupy the d_{yz} or d_{zx} orbital alternately from one V atom to its neighboring V atoms, resulting in *G*-OO. The *C*-SO is manifested as the up spin state for V-1 and V-3, and the down spin state for V-2 and V-4. Due to deviation from the cubic structure, certain degree of mixture of orbitals can be observed: for example, the small occupation of $d^{\uparrow}_{zx}$ orbital (green line) for V-1 site. Note here that, in our calculation, for each fixed structure and spin configuration the orbital polarization is fully relaxed self-consistently. The calculated electronic and

magnetic structures of YVO_3 in the intermediate temperature (100 K) phase (panel *C* in Fig. 2) can be understood in the same way as the low-temperature phase of $LaVO_3$ in terms of the same spin and orbital orderings. This can be seen from the similarity of the panel (a) to the panel (c) in Fig. 2.

For the low-temperature phase of YVO_3 (panel *B* in Fig. 2), the situation is different. The nominal electronic occupations can be understood as V-1: $d^{\uparrow}_{xy}d^{\uparrow}_{yz}$; V-2: $d^{\downarrow}_{xy}d^{\downarrow}_{zx}$; V-3: $d^{\downarrow}_{xy}d^{\downarrow}_{yz}$; V-4: $d^{\uparrow}_{xy}d^{\uparrow}_{zx}$. As for the OO and SO in the *a*-*b* plane, the present situation is the same as those of (a) and (c). However, the OO and SO along the *c* axis are different. In the present case, all the V atoms along a given *c* axis have the same orbital occupation, while those belonging to the nearest-neighbor *c* axes have different orbital occupations. For instance, the d_{yz} orbital is occupied for both V-1 and V-3 sites. This *C*-OO leads to stability of the *G*-SO through AF superexchange. Comparing $LaVO_3$ with YVO_3, we can find strong mixture of orbitals in YVO_3. This is due to the enhanced structural distortion in YVO_3 compared with $LaVO_3$. The V-O-V angles are about 157 deg in $LaVO_3$, while they are reduced to about 144 deg in YVO_3.

Similar analysis was made for all other magnetic phases of these three structures. Among several results obtained, we noticed the following interesting and possibly important feature: for a fixed crystal structure, a change in the magnetic structure will not cause any significant change in the orbital ordering. It is likely that the orbital structure is mostly determined by the specific structure distortion in the present case.

B. Optical conductivities

The results for optical conductivity are summarized in Fig. 3. Experimentally, two peak structures (α and β) are observed for $E//c$ in both compounds, with peak β located at higher energy than peak α. For $LaVO_3$, peak α has a very sharp structure at low-temperature and is significantly suppressed above the transition temperature. Peak β is quite weak and almost temperature independent. In YVO_3, on the other hand, peak β has a larger weight with strong temperature dependence and peak α is weak with only little temperature dependence. For both $LaVO_3$ and YVO_3, the $E//a$ spectra are quite broad and almost temperature insensitive.

1. $LaVO_3$ *low-temperature phase:*

For $LaVO_3$ at 10 K, the *G*-OO with *C*-SO state is the most stable state. We first analyze the case of $E//c$, where we consider the intersite transition between V-1 and V-3 as the transition dipole is along the *c* axis. The calculated optical conductivity for *C*-AF in Fig. 3 shows clearly a sharp peak corresponding to the experimental peak α. Looking back to the calculated PDOS in Fig. 2, and taking the transitions from V-1 site to other sites as examples, we can assign the sharp peak α for $E//c$ to the transition from V-1-$d^{\uparrow}_{yz}$ to V-3-$d^{\uparrow}_{yz}$ as denoted by the solid red arrow in Fig. 2. This transition is not allowed if the magnetic structure along *c* axis is AF, like in the *G*-AF and *A*-AF states, where no peak is obtained around the same position of peak α. Therefore, the peak α should be suppressed above the magnetic transition temperature as observed in experiment. On the other hand, peak β seen in experiment does not exist in the calculated spectra for *C*-AF. Since the spectral weight of peak β is very small and temperature insensitive in experiment, we speculate that this peak may come from certain component of imperfect spin ordering along the *c* axis. For example, let us reverse the spin of V-3 site in Fig. 2(a). The transition from V-1-$d^{\uparrow}_{yz}$ to V-3-$d^{\uparrow}_{yz}$ located at higher energy (denoted by the red dashed arrows in Fig. 2) will be allowed and contribute to a sharp peak near the position of peak β, as shown in the spectra for the *G*-AF and *A*-AF state for $E//c$. Before moving to YVO_3, we briefly discuss the case of $E//a$, where the intersite electronic transitions between V-1 and V-2 are important. The two transitions from V-1-$d^{\uparrow}_{xy,yz}$ to V-2-$d^{\uparrow}_{xy,yz}$ (denoted as solid blue and red arrows in Fig. 2) are allowed for the *a*-*b* plane spectra, which show a broad structure due to the broad band width of unoccupied minority spin states. These *a*-*b* plane transitions produce a structure in $E//a$ curve at the position of peak β of $E//c$ curve. Due to the doubling of transition paths, one may expect a strong *a*-*b* plane spectral weight. However, by calculating the matrix elements, the actual *a*-*b* plane spectrum is not so much weighted due to the longer bonds in the *a*-*b* plane. The shoulder in the experimental $E//a$ curve at about 1.5 eV, i.e., the energy of peak α in the $E//c$ curve may originate from the spin disordering in the *a*-*b* plane. First we note that a very tiny peak is seen at this energy in the *C*-AF ground-state configuration. This structure mainly comes from the transition from the occupied V-1-$d^{\uparrow}_{zx}$ component to a small V-2-$d^{\uparrow}_{zx}$ component just above the Fermi level. However, this structure is too weak to explain the shoulder at 1.5 eV. If the spin state between V-1 and V-2 may become parallel like in *A*-AF and FM, the transition corresponding to the red dashed arrow may become allowed and produces a peak as shown in Fig. 3.

From the above assignment, some important parameters can be estimated by using the Hartree-Fock model. The peak position of α should corresponds to energy $U-J$, and peak β corresponds to $U+J$, where U and J are on site Coulomb and exchange parameters. The estimated values for U and J are 2.2 eV and 0.6 eV from our calculations, and about 2.1 eV and 0.32 eV from experiments for $LaVO_3$. The smaller J parameter estimated from experiments may suggests the spin canting or fluctuation at elevated temperature, especially for YVO_3 as discussed below.

2. YVO_3 *at low-temperature* ($T<77$ K):

Now let us discuss the low-temperature phase of YVO_3. In this case, the *C*-OO with *G*-SO state is the most stable state. As the results, the strong peak β for $E//c$ can be explained as the transition from V-1-$d^{\uparrow}_{yz}$ to V-3-$d^{\uparrow}_{yz}$ as noted by the solid red arrow in Fig. 2(B) with energy $U+J$. This transition is not allowed for the FM coupling along the *c* axis as in the case of *C*-AF or FM state, and should show strong temperature dependence as observed in experiment. As for the small peak α, the situation for *C*-OO is different from the case of $LaVO_3$ with *G*-OO. In the present case of *C*-OO, the significant mixture of different orbitals under strongly distorted VO_6 environment is crucially important to produce this small peak α located at energy $U-J$ [corresponding to the transition as noted by the green arrow in Fig. 2(b)]. Let us explain the situation in more details. If there is no orbital

mixing (the intersite hybridization for the same orbitals still exists), d_{yz} is fully occupied and d_{zx} is empty in the majority spin state both at V-1 and V-3. The unoccupied $d^{\uparrow}_{zx}$ at V-1 hybridizes with unoccupied $d^{\uparrow}_{zx}$ (not $d^{\uparrow}_{yz}$) at V-3 to produce a small $d^{\uparrow}_{zx}$ component at V-3 site at the energy of majority spin empty state. In this case, the weight of the transition from V-1-$d^{\uparrow}_{zx}$ to V-3-$d^{\uparrow}_{zx}$ is zero because of the zero occupation of V-1-$d^{\uparrow}_{zx}$ state, and the small peak α should not exist. However, as already mentioned the orbital mixing between d_{yz} and d_{zx} is significant due to the lattice distortion and produces the partial occupation of V-1-$d^{\uparrow}_{zx}$ state [green line in Fig. 2(b)]. This will contribute to the small peak α. We should emphasize here that by keeping the *C*-OO any magnetic coupling along the *c* axis will produce a peak around α only through the orbital mixing and therefore the peak α will never be strong, in contrast to the case of $LaVO_3$. Nevertheless, those states with different orbital ordering, like the intermediate temperature phase with *G*-OO and *C*-SO, can contribute to the peak structure around α as shown in Fig. 2(c).

3. YVO_3 *at intermediate temperature* (77 K$<T<$116 K):

The observed spectra for the intermediate phase of YVO_3, which has *G*-OO and *C*-SO, is hard to be explained by our calculations. Our calculations suggest a picture similar to that of the low-temperature phase of $LaVO_3$, because the two systems have the same spin and orbital orderings. However, the observed spectra is quite similar to the low-temperature phase of YVO_3, which has different spin and orbital orderings. In particular, the observed peak β is stronger than peak α and temperature dependent, while the calculations suggest the opposite. One possible scenario to explain the observed picture is to suggest the persistence of low-temperature phase (*C*-OO and *G*-SO) at elevated temperature, or at least certain mixture of other magnetic states, like *G*-OO with *G*-SO or *G*-OO with *A*-SO states. This argument can be supported by the following facts. First, the small *J* parameter (about 0.25 eV) estimated from experiment suggests the possibility of strong canting or magnetic fluctuation at elevated temperature (100 K). Second, the recent neutron experiment[25] on this compound actually suggests the existence of *G*-type spin canting and significant reduction of magnetic moment at 100 K. Nevertheless, according to our calculations, to be able to reproduce the observed shape, substantial (more than 50 percent) mixture of low-temperature phase is required.

In conclusion, we developed the first-principles plane-wave-pseudopotential method based on LDA+U to calculate the interband optical conductivity. We calculated the anisotropic optical conductivities of $LaVO_3$ and YVO_3 for different orbital and spin ordered phases, and studied the effects of spin and orbital ordering on the anisotropy. The experimentally observed spectra for both $LaVO_3$ and YVO_3 at low-temperature can be qualitatively explained by our calculations. On the other hand, our calculation for the intermediate temperature phase for YVO_3 suggests that substantial mixture of low-temperature phase may persist at elevated temperature.

ACKNOWLEDGMENTS

The authors appreciate Professor Y. Tokura and Dr. S. Miyasaka for fruitful discussions and providing their experimental data. The authors also acknowledge the valuable discussion with Dr. I. V. Solovyev and Dr. Y. Motome.

[1] Y. Tokura and N. Nagaosa, Science **288**, 462 (2000).
[2] Z. Fang, I.V. Solovyev, and K. Terakura, Phys. Rev. Lett. **84**, 3169 (2000).
[3] Z. Fang and K. Terakura, J. Phys.: Condens. Matter **14**, 3001 (2002).
[4] Y. Murakami *et al.*, Phys. Rev. Lett. **81**, 582 (1998); **80**, 1932 (1998).
[5] Y. Okimoto *et al.*, Phys. Rev. B **59**, 7401 (1999).
[6] K. Tobe, T. Kimura, Y. Okimoto, and K. Tokura, Phys. Rev. B **64**, 184421 (2001).
[7] K.H. Ahn and A.J. Millis, Phys. Rev. B **61**, 13 545 (2000).
[8] K. Terakura, I. V. Solovyev, and H. Sawada, in *Colossal Magnetoresistive Oxides*, edited by Y. Tokura (Gordon & Breach Science Publishers, London, 2000).
[9] P. Bordet *et al.*, J. Solid State Chem. **106**, 253 (1993).
[10] S. Miyasaka, T. Okuda, and Y. Tokura, Phys. Rev. Lett. **85**, 5388 (2000).
[11] H. Kawano, H. Yoshizawa, and Y. Ueda, J. Phys. Soc. Jpn. **63**, 2857 (1994).
[12] M. Noguchi *et al.*, Phys. Rev. B **62**, R9271 (2000).
[13] G.R. Blake *et al.*, Phys. Rev. Lett. **87**, 245501 (2001); Phys. Rev. B **65**, 174112 (2002).
[14] Y. Ren *et al.*, Nature (London) **396**, 441 (1998).
[15] H. Sawada and K. Terakura, Phys. Rev. B **53**, 12 742 (1996).
[16] V.I. Anisimov, J. Zaanen, and O.K. Anderson, Phys. Rev. B **44**, 943 (1991); I.V. Solovyev, P.H. Dederichs, and V.I. Anisimov, *ibid.* **50**, 16 861 (1994).
[17] H. Sawada and K. Terakura, Phys. Rev. B **58**, 6831 (1998).
[18] S. Miyasaka, Y. Okimoto, and Y. Tokura, J. Phys. Soc. Jpn. **71**, 2086 (2002).
[19] D. Vanderbilt, Phys. Rev. B **41**, 7892 (1990).
[20] C.S. Wang and J. Callaway, Phys. Rev. B **9**, 4897 (1974).
[21] T. Fujiwara and T. Hoshi, J. Phys. Soc. Jpn. **66**, 1723 (1997).
[22] H. Kageshima, and K. Shiraishi, Phys. Rev. B **56**, 14 985 (1997).
[23] T. Arima, Y. Tokura, and J.B. Torrance, Phys. Rev. B **48**, 17 006 (1993).
[24] T. Mizokawa and A. Fujimori, Phys. Rev. B **54**, 5368 (1996); T. Mizokawa, D.I. Khomskii, and G.A. Sawatzky, *ibid.* **60**, 7309 (1999).
[25] C. Ulrich *et al.*, (unpublished).